Global Imaging of Mantle Transition Zone Seismic Discontinuities from Observations of Body-Wave Travel-Times and Rayleigh-Wave Dispersion.

E. Debayle, B. Tauzin, and G. Wittlinger,

Ecole et Observatoire de Sciences de la Terre, Centre National de la Recherche Scientifique and Université Louis Pasteur, 5 rue René Descartes, 67084 Strasbourg Cedex, France.

Email: benoit.tauzin@eost.u-strasbg.fr

Debayle
DI05-7553

Financé par ANR

Summary

We present a global study of the 410-km and 660-km seismic discontinuities from converted (P-to-S) and reflected (SS precursors) body-waves.
P-to-S converted waves (**figures 1, 2, 3 & 4**) at a seismic discontinuity d (hereafter referred as Pds) sample the mantle transition zone (MTZ) beneath the stations (**figure 1a**), which limits the global coverage, especially in oceanic areas (**figure 1b**). However, these data provide a lateral resolution of a few hundred kilometers beneath the stations, due to their relatively narrow Fresnel zone.
SS precursors phases (**figures 5, 6, 7 & 8**) sample the MTZ near the bounce point, half-way between the source and the receiver (**figure 5a**). They provide a better global coverage of the MTZ (**figure 5b**), but with a limited lateral resolution (few thousands of kilometers) compared with Pds.

Despite different sampling and horizontal resolutions, both studies show significant lateral variations in the MTZ thickness (with maximal amplitudes of ±35 km), and an overall agreement at long wavelengths (**figures 9 & 10**). The MTZ is generally found to be thick under subductions, in agreement with the previous work of Lawrence and Shearer (2006).
A NW-SE pattern of thick MTZ beneath central and north America is revealed by the Pds study, suggesting a thickening of the MTZ associated to the fossil Farallon subduction. In oceanic regions, the MTZ is generally thin or normal, and there is no clear evidence supporting a thinning of the MTZ beneath hotspots. Lateral variations remain important in regions of the mantle located away from hotspots and present subductions.

We are working to combine SS precursors with higher mode Rayleigh waves (**figures 11, 12 & 13**) in a simultaneous inversion for both the 3D distribution of SV-wave velocities and the absolute depth of seismic discontinuities. The inversion scheme is currently tested on synthetics and will be applied soon on an actual data set.

Observations of Conversions and Reflections at the Mantle Transition Zone Discontinuities

P-to-S conversions Dataset

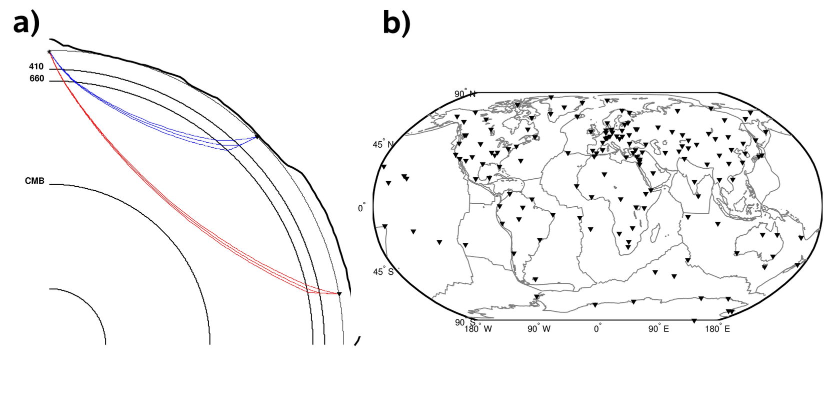

Figure 1. a) Pds ray paths after ray tracing in the IASP91 velocity model (Kennett and Engdahl,1991) for two events located at distances of 45° and 80° from the station.
b) Map showing the location of 167 FDSN stations for which we have been able to measure Pds travel-times.

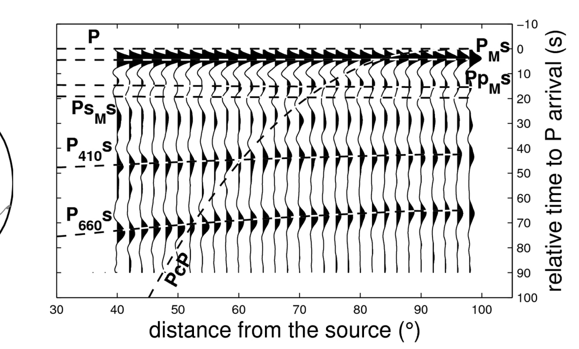

Figure 2. Section of Sv receiver functions for all our dataset.
Conversions at discontinuities (P410s and P660s) are recorded between 40° and 97° and arrive ~45 s and ~70 s after the P transmitted wave.

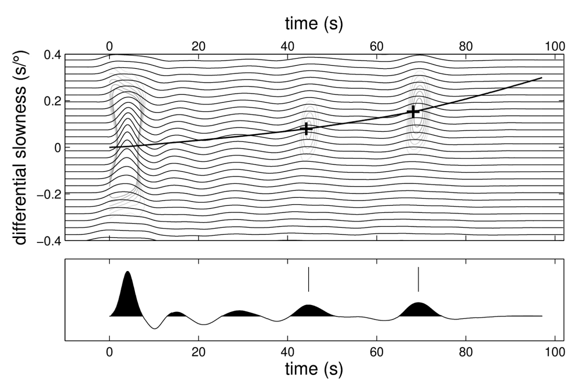

Figure 3. Stacking procedure : this example shows the slant-stack diagram obtained after stacking all our Pds dataset (**figure 2**). The seismic trace at the bottom is obtained by stacking amplitudes along the theoretical time and slowness values predicted by IASP91 (black curve on the top time-slowness diagram). The differential travel-time tP660s-tP410s is then measured on the seismic trace. We build a similar slant-stack diagram at each of the 167 stations shown in **figure 1b**.

tP660s-tP410s

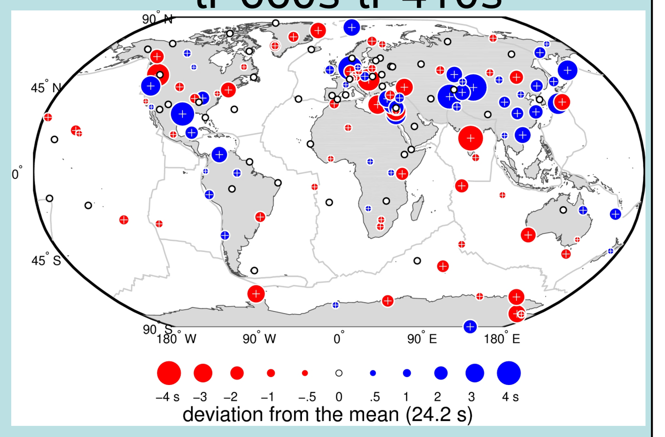

Figure 4. Differential travel-times tP660s-tP410s relative to the global average (24.2 s) obtained after applying the procedure described in **figure 3** at each of the167 stations of the **figure 1b**. Blue circles mark measurements > 0.5 s and red circles mark measurements < -0.5 s.

SS-precursors Dataset

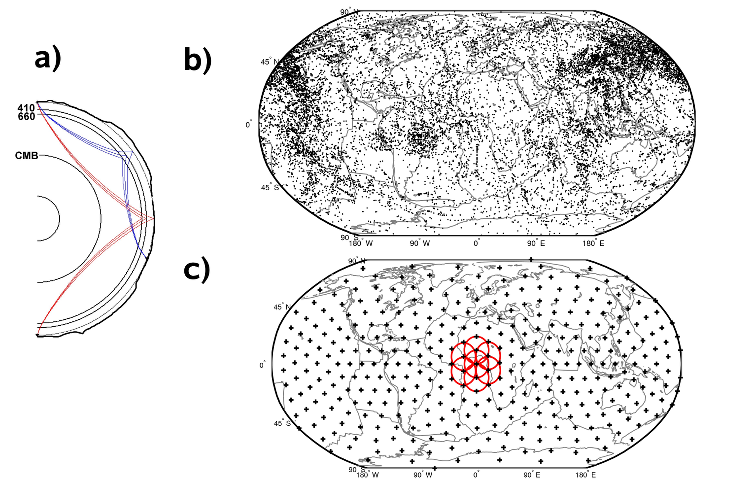

Figure 5. a) Ray paths for SS-precursors with bounce points half-way between sources and receivers.
b) Theoretical location of SS bounce points for our global dataset (17578 measurements).
c) We gather data by commun bounce points. We use 362 circular caps whose centers are marked by black crosses. A few caps are shown in red.

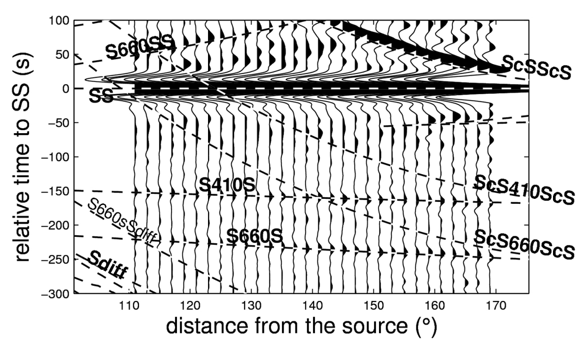

Figure 6. Seismic section of transverse components for all our global SS precursors dataset.
Underside reflections of S phases at 410-km and 660-km discontinuities (S410S and S660S) are better recorded between 110° and 170° and arrive ~-155 s and ~-230 s before the SS reference phase.

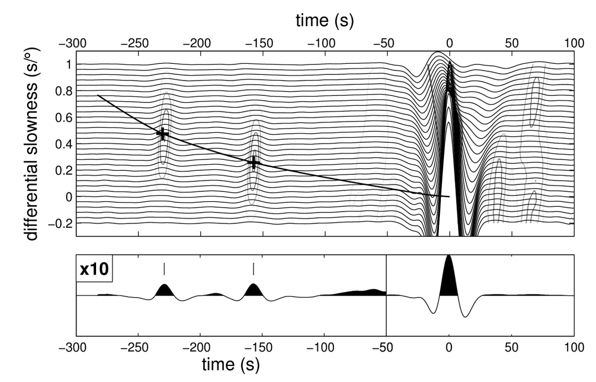

Figure 7. Stacking procedure : this example shows the slant-stack diagram obtained after satcking all our SS precursors dataset (**figure 6**). The seismic trace at the bottom is obtained by stacking amplitudes along the theoretical time and slowness values predicted by IASP91 (black curve on the top diagram). The differential travel-time tS660S-tS410S is then measured on the seismic trace. We built a similar slant-stack diagram at the 362 cap locations shown in **figure 5c**.

tS660S-tS410S

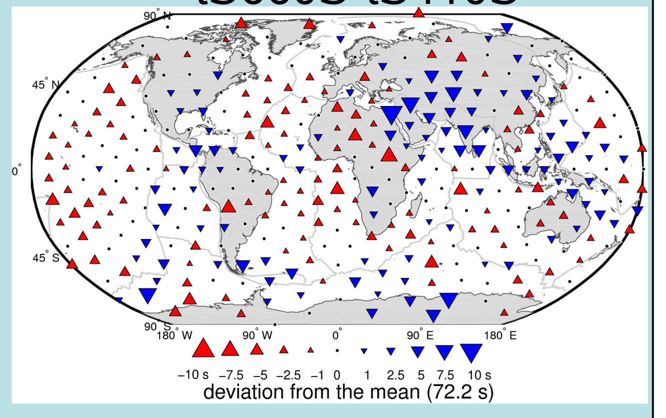

Figure 8. Differential travel-times tS660S-tS410S relative to the global average (72.2 s) obtained after applying the procedure described in **figure 7** at each of the 362 caps. Blue triangles mark measurements > 5 s and red triangles mark measurements < -5 s. Measurements are plotted at the center of each cap (**figure 1c**).

Toward a Simultaneous Inversion for Velocities and the Depth of Discontinuities

Surface-Wave Dataset

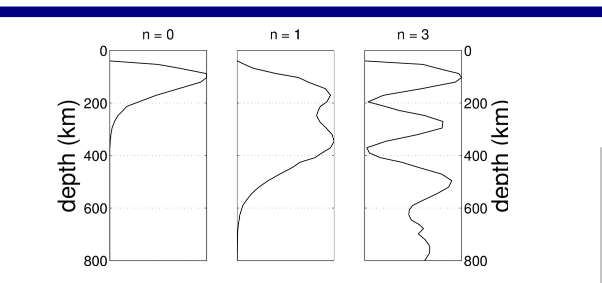

Figure 11. Sensitivity kernels for the fundamental mode (n=0), first higher mode (n=1) and third higher mode (n=3) of a Rayleigh wave at 60 s period. The curves show the partial derivatives of the phase velocity according to the shear-wave velocity for a 1 km thick layer in the PREM model.

We are working to combine SS precursors with fundamental and higher mode Rayleigh waves in a simultaneous inversion of the 3D shear-wave velocity and the depth of seismic discontinuities. Higher modes provide constraints on the background 3D shear-wave velocity structure (**figure 11**) and should help to better map the absolute depth of seismic discontinuities .

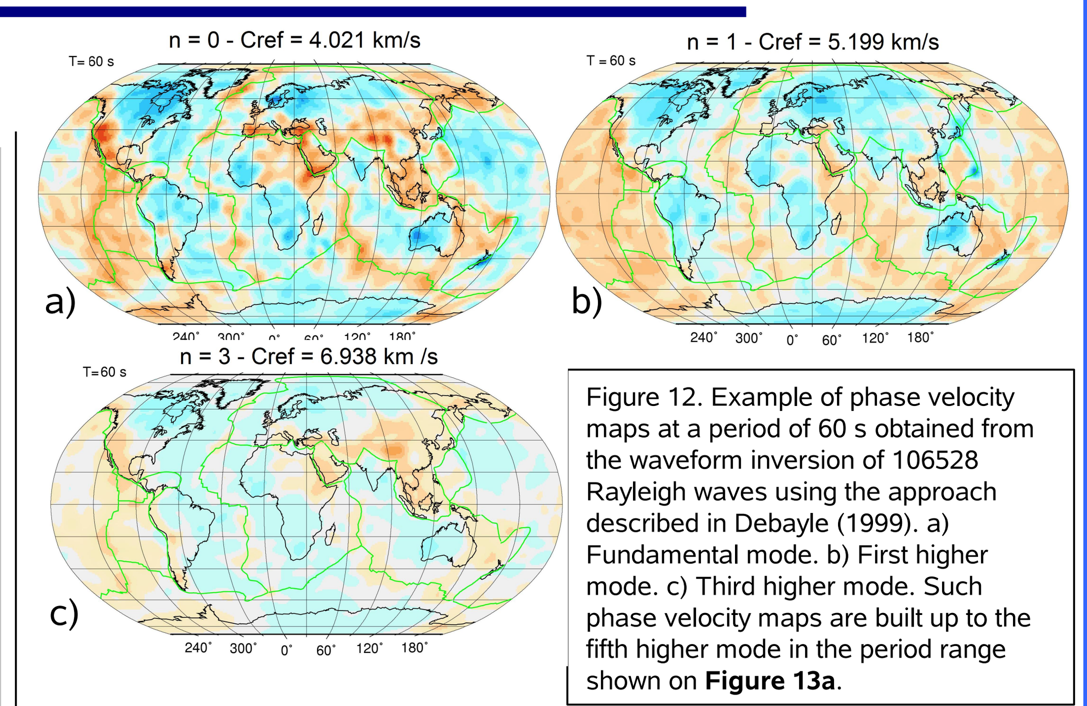

Figure 12. Example of phase velocity maps at a period of 60 s obtained from the waveform inversion of 106528 Rayleigh waves using the approach described in Debayle (1999). a) Fundamental mode. b) First higher mode. c) Third higher mode. Such phase velocity maps are built up to the fifth higher mode in the period range shown on **Figure 13a**.

Simultaneous inversion

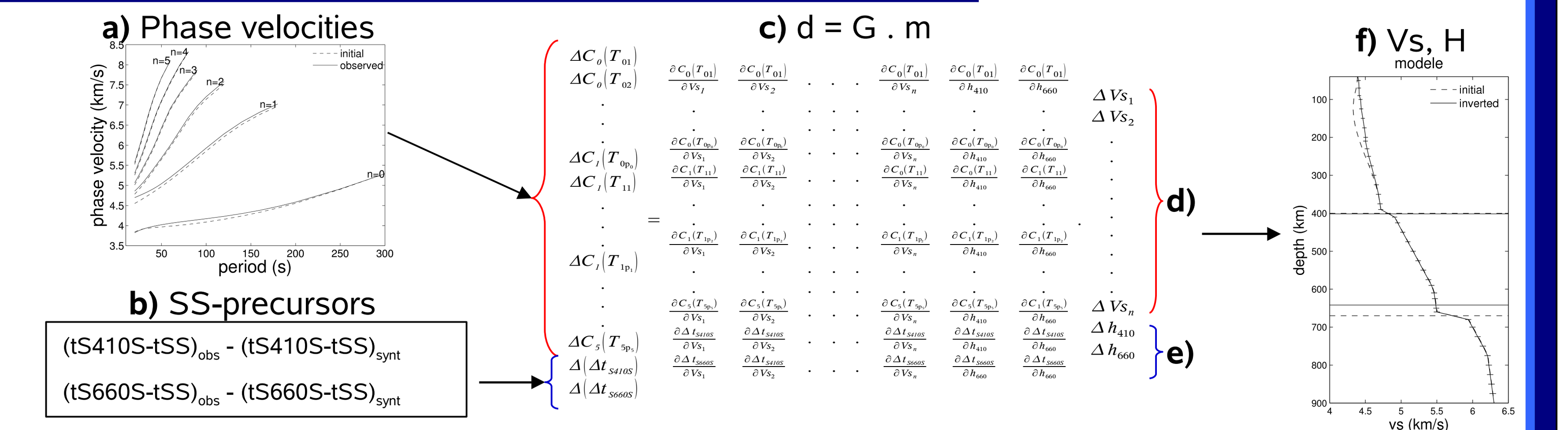

Figure 13. Principle of the simultaneous inversion scheme illustrated on a 1D example.

For each cap of **figure 5c**, we extract from our phase velocity maps (**figure 12**) a set of dispersion curves as in **figure 13a**. We can then simultaneously invert the phase velocity curves (**figure 13a**) and the SS precursors travel-times (**figure 13b**) for a local 1D profile (**figure 13f**) . The 1D profile includes perturbations of the shear-wave velocity (**figure 13d**) and of the depth of the 410-km and 660-km discontinuities (**figure 13e**). A 3D model of the shear wave velocity and topography variations is obtained from the juxtaposition of the inverted 1D models. The inversion scheme is currently tested and will be applied soon on an actual data set.

Mantle Transition Zone Thickness

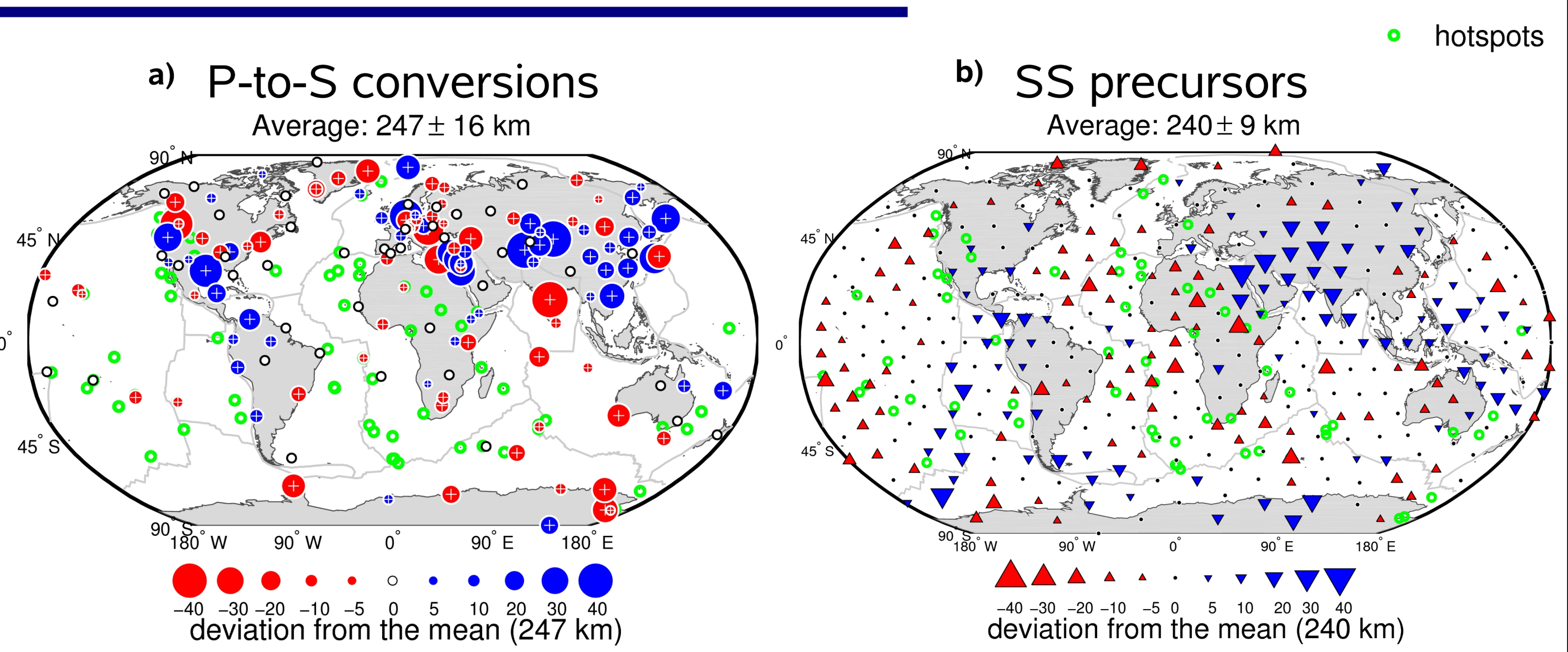

Figure 9. a) MTZ thickness obtained from observations of P-to-S converted waves. b) MTZ thickness obtained from observations of SS precursors. Our measured differential travel-times tP660s-tP410s (**figure 4**) and tS660S-tS410S (**figure 8**) have been converted into MTZ thickness using PREM (Dziewonsky and Anderson, 1981) at 20 s period. Green circles mark hotspot locations.

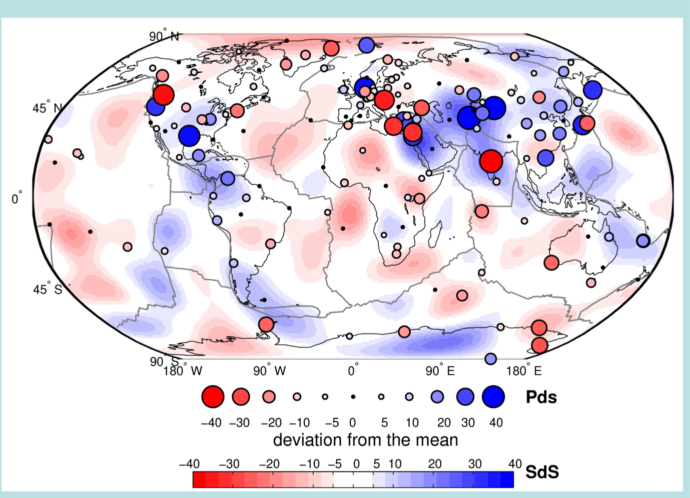

Figure 10. Comparison of the MTZ thickness variations obtained using SS precursors and P-to-S conversions. Variations are shown with respect to the global average of each dataset. SS precursors observations have been expanded on a spherical harmonic basis up to degree 12 (background colors). Blue color is for thicker MTZ and red color is for thinner MTZ. P-to-S observations are plotted with blue plain circles (> 5 km) or red plain circles (< -5 km) at each station location.

Comparison of Pds and SS precursors results

Agreement :

- Overall agreement :
  - The average MTZ thickness: 247 km for Pds (**figure 9a**) and 240 km for SdS (**figure 9b**).
  - The amplitudes of variations of the MTZ thickness: ±40 km for Pds (**figure 9a**) and ±35 km for SdS (**figure 9b**).
  - The long wavelength pattern.
- At regional scale (**figures 9 & 10**) :

THICK MTZ		THIN MTZ	
• North east Asia • Pamir Hindu Kush	• West Australia • Central America	• Erebus Mount* • Kerguelen*	• Lac Victoria* • East Australia

*** hotspots**

Disagreement (figure 10) :

MTZ under	with Pds	with SdS
• India	thin (~ -45 km)	thick (~ +15 km)
• South-East China	thick (~ +25 km)	thin (~ -10 km)
• South Pacific Superswell*	normal	thin (~ -10 km)
• Antarctic Peninsula	thin (~ -25 km)	normal

Insights on Geodynamics

Our global observations of P-to-S converted waves and SS precursors show an overall agreement at long wavelengths. We confirm the observations of a thick MTZ under a number of active subduction zones (north-west Pacific, Indonesia, Solomon, Hebridies, Peru, Chile, Pamir and Hindu Kush region). This suggests that parts of the 410-km and 660-km topography variations are due to the effect of cold subducted plates on the olivine phase transformation.
At large scale, SS precursors show that the MTZ is generally thinner in oceanic regions, but do not support a thin MTZ beneath hotspots. A detailed analysis of our Pds dataset has confirmed that for most hotspots the MTZ is not significantly thinner, although the 410-km discontinuity is generally deflected downward **(see Benoit Tauzin's talks, friday morning at 09:48h, Moscone West, room 3005)**. This is consistent with the effect of a phase transition from majorite-garnet to perovskite at a depth of 660 km, as suggested by Hirose (2002).
Lateral variations in MTZ thickness can remain important in regions of the mantle located away from hotspots and present subductions. In central and north America, the NW-SE pattern of thick MTZ observed with Pds is consistent with the SS precursors observations and suggests a thickening of the MTZ associated to the fossil Farallon subduction.

Acknowledgements

This work was supported by the program DyeTI of the Institut National des Sciences de l'Univers (INSU) at CNRS and by the young researcher ANR TOMOGLOB no ANR-06-JCJC-0060. We thank the IRIS and Geoscope data centers for providing seismological data.

References

E. Debayle, SV-wave azimuthal anisotropy in the Australian upper mantle: preliminary results from automated Rayleigh waveform inversion, *Geophys. J. Int.*, 137, 747-754, 1999.
Dziewonski, A.M, and D. Anderson (1981), Preliminary Reference Earth Model, *Phys. Earth Planet. Inter.*, 25, 297-356, doi:10.1016/0031-9201(81)90046-7.
Hirose, K. (2002), Phase transitions in pyrolitic mantle around 670-km depth: Implications for upwelling of plumes from the lower mantle, *J. Geophys. Res.*, 107, B4, doi: 10.1029/2001JB000597.
Kennett, B., Engdahl (1991), Travel times for global earthquake location and phase identification, *Geophys J Int.*, 105, 429-465.
Lawrence, J., and P. Shearer (2006), A global study of transition zone thickness using receiver functions, *J. Geophys. Res.*, 111, B06307, doi: 10.1029/2005JB003973.